

Cavity Model for the Slot Radiation of an Enclosure Excited by Printed Circuit Board Traces With Different Loads

Christian Poschalko, *Member, IEEE*, and Siegfried Selberherr, *Fellow, IEEE*

Abstract—Traces on a printed circuit board (PCB) couple to the cavity consisting of the PCB ground plane and a metallic enclosure cover. We introduce this common-mode coupling of a PCB trace to the cavity field by an analytical model that is verified with 3-D simulations using HFSS. The cavity field causes radiated emission from the slots of the cavity. For an accurate calculation of the cavity field inside the enclosure and the radiated emission, we consider the radiation loss by a multiport approach. Comparisons of the analytical results for the radiated field to measurements show good agreement. Radiated emission can be calculated for arbitrary geometric enclosure shapes as a function of frequency, position of the trace on the PCB, and trace load/driver impedances.

Index Terms—Cavity model, common-mode coupling, electrically equipped enclosures, radiated emission.

I. INTRODUCTION

CURRENT- and voltage-driven common-mode coupling have been found to be a significant source of electromagnetic radiation initiated by traces on a printed circuit board (PCB) [1]. The common-mode coupling inductance for the current-driven mode has been formulated analytically for a trace above a finite ground plane [2]–[4]. An analytical model for the voltage-driven mechanism was developed for a PCB with attached cables [5]. All formulations consider the PCB and the trace, but not the influence of an enclosure. In many applications, a metallic plane is parallel to the PCB at an electrically short distance. This plane has an influence on the common-mode coupling impedance. Examples of such applications are drives (compact disk/digital video disk), slots for 19 in racks, automotive control devices, or metallic cooling devices above a PCB. Some configurations have already been modeled with finite-difference time-domain simulation tools [6], [7].

To ensure power integrity in high-speed applications, power network design methods have been developed [9], [10] based on an analytical cavity model that can be used for fairly arbitrary shaped power planes. This cavity field model is sufficient for metallic planes that are parallel to each other over an electrically small distance. Therefore, this model can also be used to calculate the fields between the ground plane of a PCB and the metallic cover of an enclosure, as shown in Fig. 1.

Manuscript received March 11, 2008; revised August 12, 2008 and October 3, 2008. Current version published February 13, 2009. This work was supported by the Medea + Parachute Program.

C. Poschalko is with Robert Bosch AG, Diesel and Gasoline Systems, A-1110 Vienna, Austria (e-mail: christian.poschalko@chello.at).

S. Selberherr is with the Institute for Microelectronics, Technische Universitat Wien, A-1040 Vienna, Austria (e-mail: selberherr@tuwien.ac.at).

Digital Object Identifier 10.1109/TEM.2008.2008815

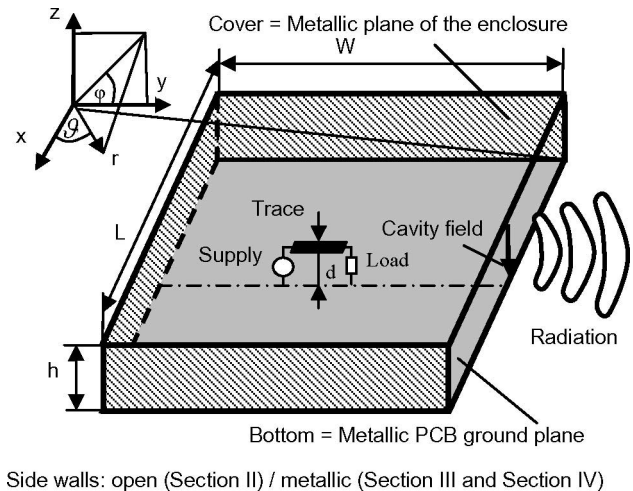


Fig. 1. Trace on the PCB couples to the cavity and causes radiation from the cavity slots. We used this spherical angle definition as it enables simpler radiation field expressions (Section IV).

The excitation in [9] and [10] has been described by ports between the upper and the lower plane. (current sources).

In the case of a PCB ground plane parallel to a metallic enclosure cover, traces between these planes couple to the cavity (Fig. 1) and the excitation is not caused by currents galvanically supplied from the upper to the lower plane.

Section II of this paper describes how traces can be introduced to cavity formulations like those in [9] and [10] by ports. An introduction of traces to the cavity field based on mode decomposition was also suggested in [8]. The method in [8] has been implemented in the commercial tool SIwave. In contrast to [8], our method introduces the trace with a simple distance rate factor without the need of mode decomposition. The advantage of the method presented here is that it is an efficient analytical solution. Our method is valid when the characteristic impedance of the trace is not influenced by the cover, which is satisfied as long as $d \ll h$. In this case, the coupling from the cavity back to the trace can be neglected. For validation, we compare HFSS transfer impedance simulations with and without the use of our trace introduction method.

Section III describes analytical formulations for the cavity field inside a cubical enclosure with a slot on one side. The base functions in these formulations are different compared to [9] and [10] because of the different boundary conditions.

In Section IV, we consider the radiation loss that has a significant influence on the cavity field. The far-field expressions

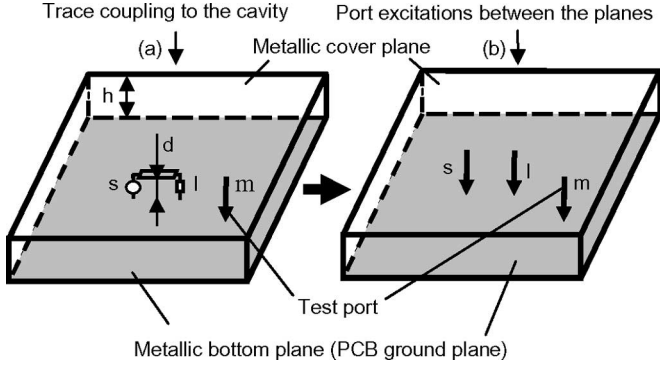


Fig. 2. Trace that couples to the parallel planes is introduced to an analytical cavity formulation like [9] and [10] by two ports at positions s and l . We use a test port m to compare the voltages of (a) and (b).

of a cavity model were calculated in [12] without consideration of the radiation loss. Later, this loss in the cavity model was introduced in [12] by a quality factor. When the radiation loss becomes the dominant loss mechanism, this method fails as the radiated power calculated from the model without the radiation loss will be significantly too high. Our approach is to introduce a loss admittance network to ports defined at the open slot of the enclosure. This method accurately considers radiation as the admittances are calculated independently of the cavity model. For validation, we present electric far-field results of our analytical model compared with HFSS simulations and measurement results.

Section V contains a summary of the results and a conclusion for applications.

II. COUPLING OF TRACES TO PLANE CAVITY FIELDS

The analytical cavity model of [9] and [10] has been derived for rectangular planes with four open sides under the following conditions:

- 1) an electrically short gap between the planes;
- 2) perfect magnetic walls at the open boundaries;
- 3) perfect electric conducting planes.

Using these conditions, only the magnetic field transversal to the z -direction, TM_{z_m} mode $m = 0$, is considered in the cavity model and the electric field has thus only a z -component. This is sufficient also in case of a trace within the cavity as higher order parallel-plate modes excited by the horizontal trace current decay rapidly and cannot reach the surrounding edges. Therefore, any horizontal current can be neglected and the vertical trace currents at the source (s) and load (l) positions (Fig. 2) couple to the cavity. Excitations are introduced to the cavity model by vertical ports between the upper and lower plane. This n -port system is described by the impedance matrix (1)

$$U_i(x_i, y_i) = \sum_{j=1}^{n\text{-port}} (Z_{ij}(x_i, y_i, x_j, y_j) \cdot I_j(x_j, y_j)). \quad (1)$$

Here, $U_i(x_i, y_i)$ is the voltage on port i , $I_j(x_j, y_j)$ is the current on port j , $Z_{ij}(x_i, y_i, x_j, y_j)$ is the impedance matrix, and n -port is the number of ports. Analytical expressions for Z_{ij} are given

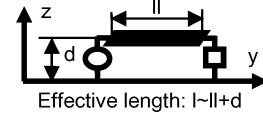


Fig. 3. Effective trace length to be used in (7).

by [9] and [10]. Fig. 2 depicts the introduction of the trace to the n -port cavity model.

The port excitation currents in Fig. 2(b) are the trace currents at s and l in Fig. 2(a) multiplied by the ratio [(distance trace to GND)/(distance cover to GND)] (d/h). The mode considered in the cavity model implies that the field does not vary in z -dimension. Therefore, one obtains a linear weighting factor d/h .

Port m in Fig. 2 has been introduced for the voltage measurement between the planes. With (1), the voltage on the test port U_m can be expressed by

$$U_m = Z_{mm} \cdot I_m + (Z_{ms} \cdot I_s + Z_{ml} \cdot I_l) \cdot d/h. \quad (2)$$

The trace voltages and currents at these positions (s , l) can be expressed by transmission line theory [Fig. 2(a)] as

$$U_s = \cosh(\gamma \cdot l) \cdot U_l - \sinh(\gamma \cdot l) \cdot I_l \cdot Z_w \quad (3)$$

$$I_s = \sinh(\gamma \cdot l) \cdot U_l / Z_w - \cosh(\gamma \cdot l) \cdot I_l. \quad (4)$$

Z_w is the characteristic impedance of the trace, γ is the complex propagation factor of the trace, and l is the trace length. The relation of the load voltage to the load current is given by the load impedance

$$Z_l = -U_l / I_l. \quad (5)$$

Equations (4) and (5) lead to

$$I_s = -(\sinh(\gamma \cdot l) \cdot Z_l / Z_w + \cosh(\gamma \cdot l)) \cdot I_l. \quad (6)$$

Since port m acts like a voltage probe, the current $I_m = 0$. With $I_m = 0$, and (2) and (6), the transfer impedance of the current at the source of the trace to the voltage on the test port becomes

$$\frac{U_m}{I_s} = \frac{d}{h} \cdot \left(Z_{ms} - Z_{ml} \left/ \left(\sinh(\gamma \cdot l) \cdot \frac{Z_l}{Z_w} + \cosh(\gamma \cdot l) \right) \right. \right). \quad (7)$$

Equation (7) describes the voltage between the two planes at the test port m for a given trace source current.

The vertical connections of the trace have to be considered by using an effective trace length l (Fig. 3) in (7).

Equation (7) provides an analytical solution for the introduction of traces to a cavity field formulation like in [9] and [10].

Therefore, the theory developed in [9] and [10] for power network design applications can also be used for the calculation of cavity fields caused by traces on a PCB, which couple to an enclosure. To prove (7), geometries (a) and (b) of Fig. 2 have been modeled in HFSS using perfect conducting sheets for the planes and lumped ports at the positions s , l , and m . Fig. 4 depicts the geometry used for the HFSS models.

HFSS is a full-wave finite-element solver that calculates the S - and Z -parameters from the ports. The Z -parameters Z_{ms} and Z_{ml} for the setup in Fig. 2(b) have been used together with

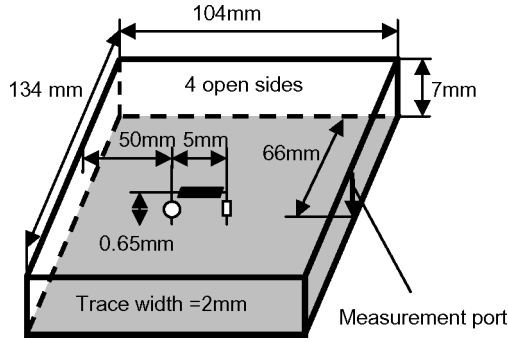


Fig. 4. Model dimensions for the results in Fig. 5.

(7) to calculate the transfer function for that case. We calculated the transfer function for the test setup in Fig. 2(a) using the Z values from this model

$$\begin{pmatrix} U_m \\ U_s \\ U_l \end{pmatrix} = \begin{pmatrix} Z_{mm_a} & Z_{ms_a} & Z_{ml_a} \\ Z_{sm_a} & Z_{ss_a} & Z_{sl_a} \\ Z_{lm_a} & Z_{ls_a} & Z_{ll_a} \end{pmatrix} \cdot \begin{pmatrix} 0 \\ I_s \\ -U_l/Z_l \end{pmatrix} \quad (8)$$

$$\frac{U_m}{I_s} = Z_{ms_a} - \frac{Z_{ml_a} \cdot Z_{ls_a}}{Z_{ll_a} + Z_l} \quad (9)$$

We used the “ $_a$ ” notation for the impedances in (8) to show that these Z parameters are obtained with the HFSS model in Fig. 2(a). Fig. 5 shows comparisons of the transfer impedances of both models in Fig. 2(a) and (b) for trace loads Z_l : 0, 50, and $1E9 \Omega$.

The HFSS simulations have been carried out with radiation boundary box walls surrounding the simulation domain. In contrast to the analytical model of [9] and [10] with perfect magnetic conducting edges of the cavity, the edges in the HFSS model could radiate. The HFSS simulations were used to show that our method of introducing the trace to the cavity by (7) is correct also in this practically relevant case of radiation from the cavity edges. The characteristic impedance of the trace has been calculated following [14], without considering the cover plane of the enclosure, which is possible if $d \ll h$ (Fig. 1)

$$Z_w = 60 \cdot \ln \left[\frac{f_1(w/h)}{w/h} + \sqrt{1 + \left(\frac{2 \cdot h}{w} \right)^2} \right]$$

$$f_1 = 6 + (2 \cdot \pi - 6) \cdot \exp \left[- (30.666 \cdot h/w)^{0.7528} \right]. \quad (10)$$

Here, w is the trace width. This model does not consider any dielectric material. In any practical application, the dielectric properties of the PCB have to be taken into account, with appropriate formula for the characteristic impedance and effective lengths for d and h .

III. ANALYTICAL CAVITY FIELD FORMULATION FOR A SLIM ENCLOSURE WITH A SLOT ON ONE SIDE

The cavity model of [9] and [10] considers two rectangular planes with perfect magnetic wall boundaries on each side. We obtained the cavity model for the enclosure depicted in Fig. 1

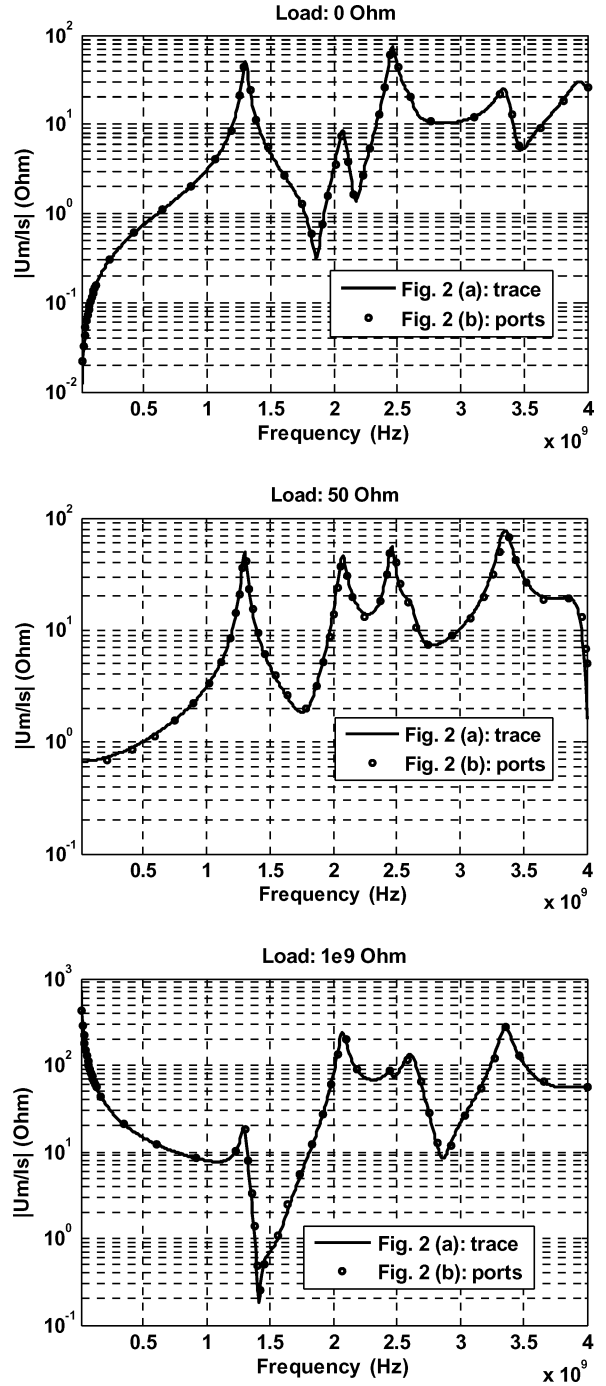


Fig. 5. Comparisons of the HFSS model with a trace in Fig. 2(a) and with ports in Fig. 2(b). U_m is the voltage at the test port and I_s the source current.

using the same separation method as in [9] and [10], but with the following boundary conditions for the plane edges:

$$\begin{aligned} x = 0 \ \& \ x = L \quad \text{PEC walls } E_z = 0 \Rightarrow X(x) = 0 \\ \Rightarrow B_m &= 0 \ \& \ k_m \cdot L = m \cdot \pi \\ y = 0 \quad \text{PEC walls } E_z &= 0 \Rightarrow Y(y) = 0 \\ \Rightarrow D_n &= 0 \end{aligned}$$

$$\begin{aligned}
 y = W \quad \text{PMC walls} \quad \frac{\partial E_z}{\partial y} = 0 &\Rightarrow \frac{\partial Y(y)}{\partial y} = 0 \\
 \Rightarrow k_n \cdot W = \frac{(2 \cdot n + 1)}{2} \cdot \pi
 \end{aligned}$$

where a perfect electrically conducting boundary is represented by PEC and a perfect magnetically conducting boundary by PMC.

With these boundary conditions, the impedances in Z_{ij} in (1) become

$$Z_{ij} = \frac{j \cdot \omega \cdot \mu_0 \cdot h}{L \cdot W} \cdot \sum_{m=0}^{\infty} \sum_{n=0}^{\infty} \left\{ \frac{4}{k_{x,m}^2 + k_{y,n}^2 - k^2} \cdot \sin(k_{x,m} \cdot x_i) \cdot \sin(k_{y,n} \cdot y_i) \cdot \sin(k_{x,m} \cdot x_j) \cdot \sin(k_{y,n} \cdot y_j) \right\}. \quad (11)$$

Here, x_i, y_i and x_j, y_j are the positions of ports i and j , respectively, and

$$k_{x,m} = \frac{m \cdot \pi}{L}, \quad k_{y,n} = \frac{(2 \cdot n + 1) \cdot \pi}{W}, \quad k = \frac{\omega}{c_l}. \quad (12)$$

Here, c_l is the speed of light for vacuum. With (7) and (11), the parallel-plane voltage initiated by trace coupling inside an enclosure like Fig. 1 can be calculated analytically.

For an enclosure like in Fig. 1, the fringing fields at the slot have to be considered by using $We = W + h/4$ instead of W in (11) and (12). In [12], $We = W + h/2$ has been taken to consider the fringing fields for planes with two open boundaries associated with dimension W , but as the enclosure in Fig. 1 has only one open edge, the correction must be performed by using $We = W + h/4$. An additional correction has to be carried out to consider the wall thickness d_w of the enclosure.

This is not necessary in the case of power planes on a PCB as the conducting layers are thin; however, a metallic enclosure usually has thicker walls. To consider a nonnegligible wall thickness of the enclosure, $We = W + h/4 + d_w$ has been used for the calculation.

Perfect electrically conducting planes, air in the cavity, and a PMC at the slot have been used to derive our formulation, neglecting any losses that lead to significant deviations at the resonance frequencies compared to a real lossy situation.

An enclosure (Fig. 1) has usually a much higher plane separation h than power-ground planes on a PCB. Therefore, the radiation loss becomes the dominant loss mechanism [11]–[13] and must be considered in the cavity model to obtain a reasonable good solution.

IV. CONSIDERATION OF THE RADIATION LOSS AND RADIATED FAR FIELD

We introduce a loss admittance network to ports defined at the open slot of the enclosure (Fig. 1) in order to consider the radiation loss. This admittance network is calculated independently of the cavity model. Therefore, the solution of (1) and (11) with this admittance network includes the correct radiation loss.

In the case of an enclosure with one open slot, the far-field components can be calculated by the equivalent source method in the same way as shown for four open boundaries in [11]. This

leads to the following expressions for the far-field

$$\vec{E} = -\frac{j \cdot k}{4 \cdot \pi} \cdot \frac{e^{-j \cdot k \cdot r}}{r} \cdot \sin(\vartheta) \cdot \vec{e}_\varphi \cdot \int_{x=0}^L U(x) \cdot e^{j \cdot k \cdot x \cdot \cos(\vartheta)} \cdot dx \quad (13)$$

$$\vec{H} = -\frac{j \cdot k^2}{4 \cdot \pi} \cdot \frac{e^{-j \cdot k \cdot r}}{r} \cdot \frac{1}{\omega \cdot \mu} \cdot \sin(\vartheta) \cdot \vec{e}_\vartheta \cdot \int_{x=0}^L U(x) \cdot e^{j \cdot k \cdot x \cdot \cos(\vartheta)} \cdot dx. \quad (14)$$

Equations (13) and (14) are valid for the far-field region. The distance r must satisfy the following condition [15]:

$$r \geq (2 \cdot L^2) / \lambda_0. \quad (15)$$

Here, λ_0 is the wavelength in the air. The slot face is divided into p equidistant sections. Each section is one port and we assume that the voltage is constant along one port. With this segmentation of the slot, we write the far-field initiated by the port voltages as a summation

$$\vec{E} = -\frac{j \cdot k}{4 \cdot \pi} \cdot \frac{e^{-j \cdot k \cdot r}}{r} \cdot \sin(\vartheta) \cdot \vec{e}_\varphi \cdot \frac{L}{p} \cdot \sum_{i=1}^p \{U_{p-i} \cdot \exp(j \cdot k \cdot x_i \cdot \cos(\vartheta))\}. \quad (16)$$

$$\vec{H} = -\frac{j \cdot k^2}{4 \cdot \pi} \cdot \frac{e^{-j \cdot k \cdot r}}{r} \cdot \frac{1}{\omega \cdot \mu} \cdot \sin(\vartheta) \cdot \vec{e}_\vartheta \cdot \frac{L}{p} \cdot \sum_{i=1}^p \{U_{p-i} \cdot \exp(j \cdot k \cdot x_i \cdot \cos(\vartheta))\}. \quad (17)$$

Here, p is the number of ports at the slot, defined equidistantly along the slot with length L , x_i is the x -position at the slot of the port with index i . The radiated power density in the far-field is given by

$$\vec{S} = \vec{E} \times \vec{H}^*. \quad (18)$$

We introduce (16) and (17) into (18), and from the multiplication of the summation terms, we obtain the mutual and self-pointing vectors from the different ports. As an example for ports c and r , this pointing vector is

$$\vec{S}_{cr} = \frac{k^3}{16 \cdot \pi^2} \cdot \frac{1}{\omega \cdot \mu} \cdot \sin^2(\vartheta) \cdot \vec{e}_r \cdot \left(\frac{L}{p}\right)^2 \cdot U_c \cdot U_r^* \cdot \exp(j \cdot k \cdot (x_c - x_r) \cdot \cos(\vartheta)). \quad (19)$$

Here, x_c is the x -position at the slot of the port with index c , and x_r is the x -position at the slot of port with index r . Equation (19) is integrated over the sphere to obtain the pointing power S_{cr} from slot port at x_r to that at x_c

$$S_{cr} = \frac{k^3}{8 \cdot \pi \cdot \omega \cdot \mu} \cdot U_c \cdot U_r^* \cdot \left(\frac{L}{p}\right)^2 \cdot \int_{\vartheta=0}^{\pi} \sin^3(\vartheta) \cdot \exp[j \cdot k \cdot (x_c - x_r) \cdot \cos(\vartheta)] \cdot d\vartheta. \quad (20)$$

We obtain the mutual admittance of the two ports c and r by relating this far-field power to the voltages at the slot ports

$$Y_{a-cr} = \frac{S_{cr}}{U_c \cdot U_r^*} = \frac{k^3}{8 \cdot \pi \cdot \omega \cdot \mu} \cdot \left(\frac{L}{p}\right)^2 \cdot \int_{\vartheta=0}^{\pi} \sin^3(\vartheta) \cdot \exp[j \cdot k \cdot (x_c - x_r) \cdot \cos(\vartheta)] \cdot d\vartheta. \quad (21)$$

Here, \mathbf{Y}_a denotes the admittance matrix and Y_{a-cr} is the matrix element with indexes c (column), r (row).

Note that Y_{a-cr} is independent of the slot port voltages. Therefore, the matrix \mathbf{Y}_a can be introduced to the cavity model to obtain the correct radiation loss. The electric field (16) and the magnetic field (17) have only one vector component in the spherical coordinate system, defined in Fig. 1. Equation (21) is also much simpler with this coordinate system definition, compared to the commonly used definition. The number of ports p , which is necessary to achieve certain accuracy, depends on the maximum frequency. A calculation with increased p can be carried out to check, whether p is sufficiently high. The relation of the port voltages to the port currents is given by the impedance matrix

$$\begin{pmatrix} U_m \\ U_s \\ U_l \\ U_1 \\ \vdots \\ U_p \end{pmatrix} = \begin{pmatrix} Z_{mm} & Z_{ms} & Z_{ml} & Z_{mp1} & \cdots & Z_{mpn} \\ Z_{sm} & Z_{ss} & Z_{sl} & Z_{sp1} & \cdots & Z_{spn} \\ Z_{lm} & Z_{ls} & Z_{ll} & Z_{lp1} & \cdots & Z_{lpn} \\ Z_{1m} & Z_{1s} & Z_{1l} & Z_{1p1} & \cdots & Z_{1pn} \\ \vdots & \vdots & \vdots & \vdots & \vdots & \vdots \\ Z_{pm} & Z_{ps} & Z_{pl} & Z_{p1} & \cdots & Z_{pp} \end{pmatrix} \cdot \begin{pmatrix} I_m \\ I_s \\ I_l \\ I_1 \\ \vdots \\ I_p \end{pmatrix}. \quad (22)$$

The port voltages are U_m at the test port (at the slot), U_s at the source port inside the enclosure, U_l at the load port inside the enclosure, and U_i (i ranging from 1 to p) at the interface ports at the slot.

The port currents are I_m at the voltage test port ($I_m = 0$), I_s at the source port inside the enclosure, I_l at the load port inside the enclosure, and I_i (where i ranges from 1 to p) at the interface ports at the slot.

Matrix notation gives

$$\begin{pmatrix} U_1 \\ \vdots \\ U_p \end{pmatrix} = \begin{pmatrix} Z_{1s} & Z_{1l} \\ \vdots & \vdots \\ Z_{ps} & Z_{pl} \end{pmatrix} \cdot \begin{pmatrix} I_s \\ I_l \end{pmatrix} + \begin{pmatrix} Z_{11} & \cdots & Z_{1p} \\ \vdots & \vdots & \vdots \\ Z_{p1} & \cdots & Z_{pp} \end{pmatrix} \cdot \begin{pmatrix} I_1 \\ \vdots \\ I_p \end{pmatrix} \quad (23)$$

$$\mathbf{U}_p = \mathbf{Z}_{ps} \cdot \mathbf{I}_s + \mathbf{Z}_{pp} \cdot \mathbf{I}_p$$

$$U_m = (Z_{ms} \ Z_{ml}) \cdot \begin{pmatrix} I_s \\ I_l \end{pmatrix} + (Z_{m1} \cdots Z_{mp}) \cdot \begin{pmatrix} I_1 \\ \vdots \\ I_p \end{pmatrix} \quad (24)$$

$$\mathbf{U}_m = \mathbf{Z}_{ms} \cdot \mathbf{I}_s + \mathbf{Z}_{mp} \cdot \mathbf{I}_p.$$

The relation of the voltage vector \mathbf{U}_p and the current vector \mathbf{I}_p at the interface ports is given by the admittance matrix (21)

$$\mathbf{U}_p = -(\mathbf{Y}_a)^{-1} \cdot \mathbf{I}_p. \quad (25)$$

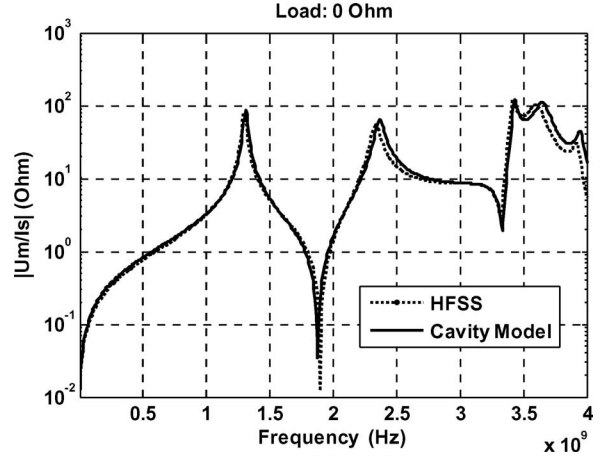


Fig. 6. Transfer function from the trace source current to the voltage on the test port. Comparison of our cavity model results to HFSS simulation results.

This leads to the final formulation for the voltage on the test port

$$\mathbf{U}_m = (\mathbf{Z}_{ms} - \mathbf{Z}_{mp} \cdot (\mathbf{Z}_{pp} + (\mathbf{Y}_a)^{-1})^{-1} \cdot \mathbf{Z}_{ps}) \cdot \mathbf{I}_s \quad (26)$$

and the voltages on the interface ports

$$\mathbf{U}_p = (\mathbf{Y}_a)^{-1} \cdot (\mathbf{Z}_{pp} + (\mathbf{Y}_a)^{-1})^{-1} \cdot \mathbf{Z}_{ps} \cdot \mathbf{I}_s. \quad (27)$$

When the radiation loss becomes very low, \mathbf{Y}_a is almost singular. For a nearly singular \mathbf{Y}_a , (26) and (27) can be simplified to avoid matrix inversion in such a case

$$\mathbf{U}_m = \mathbf{Z}_{ms} \cdot \mathbf{I}_s \quad (28)$$

$$\mathbf{U}_p = \mathbf{Z}_{ps} \cdot \mathbf{I}_s. \quad (29)$$

As (28) and (29) neglect the radiation loss, these equations may only be used at frequencies where \mathbf{Y}_a is nearly singular.

The internal enclosure voltage between the cover and the ground plane is modeled accurately by (26) and (28). To show this, we calculated the transfer impedance of the trace current to the test port voltage (geometry in Fig. 4) with (26) and (28) and 0 Ω trace load, and compared the results to HFSS (Fig. 6).

For validation of our method, we compare the electric far-field, obtained by (16) with the slot voltages from (27), to HFSS simulations and measurement results in Fig. 7. We performed the comparison on an enclosure with the geometric dimensions in Fig. 4, and for 0, 50, and 1E9 Ω as trace loads. The measurements have been carried out with a horn antenna (Amplifier Research AT4002A) and a vector network analyzer (Rhode & Schwarz ZVB4), inside an anechoic chamber. The electric field was calculated and measured 1 m in front of the enclosure slot. This position has been selected as the main lobe of the electric field distribution is oriented in this direction for some of the resonance frequencies within the evaluated range of 800 MHz to 4 GHz. The position is consistent to CISPR 25 Ed 3/CDV IEC for automotive component emission measurements above 1 GHz.

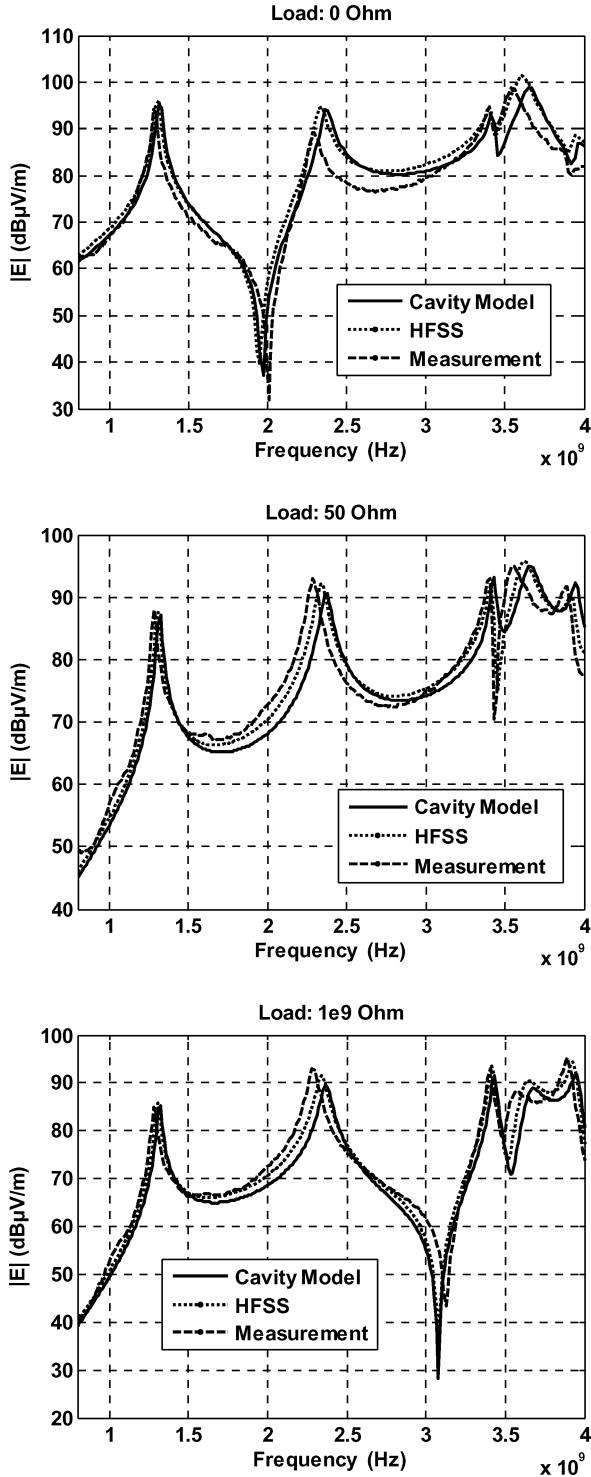


Fig. 7. Electric far-field, 1 m in front of the enclosure slot. Comparison of our cavity model results to HFSS simulation results and measurement results.

The comparison (Fig. 7) shows a reasonably good agreement of our cavity model (16) and (27) to measurement results. Equation (16) only considers the radiation from the enclosure slot and neglects the metallic enclosure walls that have some influence on the radiation diagram above the first resonance frequency. Therefore, (16) can be used to obtain a good, first-order information about the radiated field.

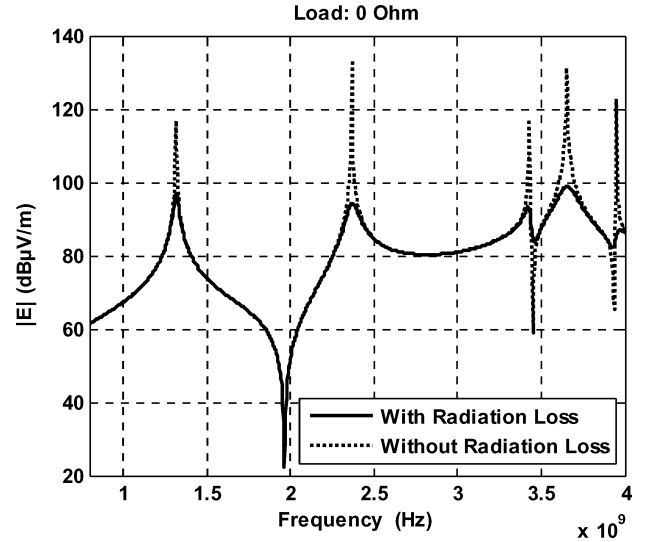


Fig. 8. Electric far-field, 1 m in front of the enclosure slot. Comparison of our cavity model results, which includes the radiation loss by introducing the admittance matrix \mathbf{Y}_a , to the results obtained from a cavity field that does not consider the radiation loss.

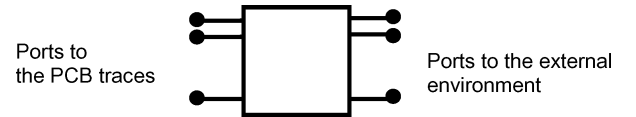


Fig. 9. Coupling path model inside the enclosure.

The consideration of the radiation loss for the calculation of the slot voltages is crucial to obtain the correct radiated far-field. Fig. 8 shows a comparison of the electric far-field obtained with our method considering the radiation loss to a lossless cavity model.

We carried out the comparisons in Figs. 5 and 7 for different trace loads to show that our model is sufficient for arbitrary load condition. The currents on the traces of a PCB can be calculated for real devices by using transmission line theory and I/O buffer information specification models [16]. Later, these currents can be used to calculate the fields inside the enclosure and the radiated emission using our cavity model.

The ports on the open slot of the enclosure establish an interface to the exterior of the enclosure. The description of the field inside the enclosure is not changed (1). Equation (1) can be interpreted as a coupling path description that is independent of the exterior of the enclosure.

This coupling path description is also valid in case of external components that have an influence on the radiation (i.e., cables). In such a case, the admittance network (matrix), which has to be connected to the coupling path ports, will change, but not the coupling path formulation. Fig. 9 depicts the interpretation of (1) as a coupling path model from traces on the PCB to the external environment interface at the slot.

V. CONCLUSION

It has been shown that the cavity field between two parallel planes excited by trace coupling can be calculated by the

introduction of two ports at the ends of the trace. Cavity field expressions are obtained for common use in power network design applications.

The theory developed for power network design can also be used to calculate the common-mode emissions caused by traces whenever a metallic plane is located at an electrically small distance above the trace.

The cavity field formulation is independent of the trace and the exterior of the enclosure. Therefore, it can be interpreted as a coupling path description that is determined by the geometry of the enclosure and the connections of the enclosure to the ground plane. This enables the enclosure to be optimized independent of the PCB layout and the exterior. The currents on the PCB traces can be calculated separately with a network simulation program. These currents can be used to calculate the common-mode radiation of very complex devices, especially as linearity enables the use of superposition.

The introduction of the trace to the cavity field formulation is performed by currents that are calculated without the influence of the enclosure. These currents are directly related to the magnetic near-field above the trace, which can be measured using a near-field scan above the PCB without the enclosure. This gives evidence for the significance of such near-field scan measurements for electromagnetic compatibility purposes.

REFERENCES

- [1] D. M. Hockanson, J. L. Drewniak, T. H. Hubing, T. P. Van Doren, F. Sha, and M. J. Wilhelm, "Investigation of fundamental EMI source mechanisms driving common-mode radiation from printed circuit boards with attached cables," *IEEE Trans. Electromagn. Compat.*, vol. 38, no. 4, pp. 557–566, Nov. 1996.
- [2] T. H. Hubing, T. P. Van Doren, and J. L. Drewniak, "Identifying and quantifying printed circuit board inductance," in *Proc. IEEE Int. Symp. Electromagn. Compat.*, Chicago, IL, Aug. 1994, pp. 205–208.
- [3] D. M. Hockanson, J. L. Drewniak, T. H. Hubing, T. P. Van Doren, F. Sha, C.-W. Lam, and L. Rubin, "Quantifying EMI resulting from finite-impedance reference planes," *IEEE Trans. Electromagn. Compat.*, vol. 39, no. 4, pp. 286–297, Nov. 1997.
- [4] M. Leone, "Design expressions for the trace-to-edge common-mode inductance of a printed circuit board," *IEEE Trans. Electromagn. Compat.*, vol. 43, no. 4, pp. 667–671, Nov. 2001.
- [5] H.-W. Shim and T. H. Hubing, "Model for estimating the radiated emissions from a printed circuit board with attached cables due to voltage-driven sources," *IEEE Trans. Electromagn. Compat.*, vol. 47, no. 4, pp. 899–907, Nov. 2005.
- [6] D. M. Hockanson, J. L. Drewniak, T. H. Hubing, and T. P. Van Doren, "FDTD modeling of common-mode radiation from cables," *IEEE Trans. Electromagn. Compat.*, vol. 38, no. 3, pp. 376–387, Aug. 1996.
- [7] D. M. Hockanson, X. Ye, J. L. Drewniak, T. H. Hubing, T. P. Van Doren, and R. E. DuBroff, "FDTD and experimental investigation of EMI from stacked-card PCB configurations," *IEEE Trans. Electromagn. Compat.*, vol. 43, no. 1, pp. 1–10, Feb. 2001.
- [8] J. E. Bracken, S. Poltyanko, S. Raman, and Z. J. Cendes, "Efficient full-wave simulation of high-speed printed circuit boards and electronic packages," in *Proc. IEEE Antennas Propag. Soc. Int. Symp. 2004*, Jun. 20–25, vol. 3, pp. 3301–3304.
- [9] G.-T. Lei, R. W. Techentin, and B. K. Gilbert, "High-frequency characterization of power/ground-plane structures," *IEEE Trans. Microw. Theory Tech.*, vol. 47, no. 5, pp. 562–569, May 1999.
- [10] C. Wang, J. Mao, G. Sellì, S. Luan, L. Zhang, J. Fan, D. J. Pommerenke, R. E. DuBroff, and J. L. Drewniak, "An efficient approach for power delivery network design with closed-form expressions for parasitic interconnect inductances," *IEEE Trans. Adv. Packag.*, vol. 29, no. 2, pp. 320–334, May 2006.
- [11] M. Leone, "The radiation of a rectangular power-bus structure at multiple cavity-mode resonances," *IEEE Trans. Electromagn. Compat.*, vol. 45, no. 3, pp. 486–492, Aug. 2003.
- [12] R. L. Chen, J. Chen, T. H. Hubing, and W. Shi, "Via coupling within power-return plane structures considering the radiation loss," in *Proc. Int. Symp. Electromagn. Compat. 2004 (EMC 2004)*, Aug. 9–13, vol. 2, pp. 386–391.
- [13] H.-W. Shim and T. H. Hubing, "A closed-form expression for estimating radiated emissions from the power planes in a populated printed circuit board," *IEEE Trans. Electromagn. Compat.*, vol. 48, no. 1, pp. 74–81, Feb. 2006.
- [14] O. Zinke and H. Brunswig, "Mikrostreifenleitung (microstrip)," in *Hochfrequenztechnik 1*, 6th ed. New Berlin, Germany: Springer-Verlag, 2000, pp. 164–168.
- [15] C. A. Balanis, "Fundamental parameters of antennas," in *Antenna Theory*, 3rd ed. New York: Wiley, 2005.
- [16] *I/O Buffer Information Specification (IBIS)*, Version 3.2, ANSI/IEA-656-A, Aug. 1999.



Christian Poschalko (M'08) was born in Austria in 1971. He received the Diplomingenieur degree in electrical engineering from Technische Universität Wien, Vienna, Austria, in 1995.

From 1996 to 1998, he was with Ernst Krause & Company as a Software Engineer for industrial automation systems. In 1998, he joined Robert Bosch AG, Vienna, where he is currently engaged in research on electromagnetic compatibility simulation of automotive control devices and for the development of simulation methods. His current research interests include electromagnetic simulation methods and electromagnetic compatibility in high-speed and power electronic systems.



Siegfried Selberherr (M'79–SM'84–F'93) was born in Austria in 1955. He received the Diplomingenieur degree in electrical engineering and the Doctoral degree in technical sciences from Technische Universität Wien, Vienna, Austria, in 1978 and 1981, respectively.

He has been holding the "venia docendi" on computer-aided design since 1984. Since 1988, he has been the Chair Professor of the Institute for Microelectronics, Technische Universität Wien. From 1998 to 2005, he served as the Dean of the Fakultät für Elektrotechnik und Informationstechnik. His current research interests include modeling and simulation of problems for microelectronics engineering.